

Article

DFT Investigations of the Reaction Mechanism of Dimethyl Carbonate Synthesis from Methanol and CO on Various Cu Species in Y Zeolites

Yuan Zhou ^{1,2}, Guoqiang Zhang ¹, Ya Song ¹, Shirui Yu ¹, Jingjing Zhao ¹ and Huayan Zheng ^{1,*} ¹ Department of Food Science and Engineering, Moutai Institute, Renhuai 564502, China² Experimental Training Teaching Center, Moutai Institute, Renhuai 564502, China

* Correspondence: andyzheng1109@163.com

Abstract: In this study, a density functional theory method is employed to investigate the reaction mechanisms of dimethyl carbonate (DMC) formation, through oxidative carbonylation of methanol, on four types of Y zeolites doped with Cu⁺, Cu²⁺, Cu₂O and CuO, respectively. A common chemical route is found for these zeolites and identified as, first, the adsorbed CH₃OH is oxidized to CH₃O species; subsequently, CO inserts into CH₃O to CH₃OCO, which reacts with CH₃O to form DMC rapidly; and finally, the adsorbed DMC is released into the gas phase. The rate-limiting step on Cu²⁺Y zeolite is identified as oxidation of CH₃OH to CH₃O with activation barrier of 66.73 kJ·mol⁻¹. While for Cu⁺Y, Cu₂O-Y and CuO-Y zeolites, the rate-limiting step is insertion of CO into CH₃O, and the corresponding activation barriers are 63.73, 60.01 and 104.64 kJ·mol⁻¹, respectively. For Cu⁺Y, Cu²⁺Y and Cu₂O-Y zeolites, adsorbed CH₃OH is oxidized to CH₃O with the presence of oxygen, whereas oxidation of CH₃OH on CuO-Y is caused by the lattice oxygen of CuO. The order of catalytic activities of these four types of zeolites with different Cu states follows Cu⁺Y ≈ Cu₂O-Y > Cu²⁺Y > CuO-Y zeolite. Therefore, CuY catalysts with Cu⁺ and Cu₂O as dominated Cu species are beneficial to the formation of DMC.

Keywords: dimethyl carbonate; Y zeolite; Cu states; density functional theory; reaction mechanism

Citation: Zhou, Y.; Zhang, G.; Song, Y.; Yu, S.; Zhao, J.; Zheng, H. DFT Investigations of the Reaction Mechanism of Dimethyl Carbonate Synthesis from Methanol and CO on Various Cu Species in Y Zeolites. *Catalysts* **2023**, *13*, 477. <https://doi.org/10.3390/catal13030477>

Academic Editor: C. Heath Turner

Received: 30 January 2023

Revised: 22 February 2023

Accepted: 24 February 2023

Published: 26 February 2023



Copyright: © 2023 by the authors. Licensee MDPI, Basel, Switzerland. This article is an open access article distributed under the terms and conditions of the Creative Commons Attribution (CC BY) license (<https://creativecommons.org/licenses/by/4.0/>).

1. Introduction

Dimethyl carbonate (DMC), which is considered as one of the environmentally benign chemicals, has been used as a low toxicity solvent and fuel additive. Its production and utilization have recently drawn much attention [1–7]. Meanwhile, DMC synthesis by oxidative carbonylation of methanol is suggested since phosgene is not produced during the process [7–11]. CuO and Cu₂O are p-type semiconductors with a direct band gap of 1.2 and 2.0 eV, respectively, which has been widely used as sensors and active centers in various catalytic reactions due to their unique electronic structure [12–14]. Similarly, Cu-exchanged zeolite catalysts, as the chloride-free catalysts, have been considered as one of the most attractive catalysts for DMC synthesis in recent years [15–19], due to the high catalytic activity and selectivity. CuY zeolite catalyst is one of them [17–23].

The presence of different Cu states in CuY zeolites results in distinct catalytic activities and is achieved using different methods. King [20] reported that Cu⁺Y zeolite prepared by solid-state ion exchange showed a satisfying catalytic activity in the oxidative carbonylation reaction, while ion-exchanged Cu²⁺Y zeolite exhibited a poor performance. Cu⁺ and CuO based Cu-FAU catalysts were prepared by Kieger et al. via ion-exchanged method and incipient-wetness-impregnation, respectively. After characterized by UV-VIS, IR, TPR and NH₃-TPD, it was suggested that Cu⁺ and CuO were formed in Cu-FAU by ion-exchange method and incipient-wetness impregnation, respectively, and Cu⁺ exhibited a better catalytic activity than CuO [24]. Richter and co-workers showed that CuO was formed in CuY zeolite when the Cu loading was above 10 wt% during incipient-wetness impregnation [25]. They pointed out that, due to the formation of CuO_x particles, oxidative carbonylation of methanol proceeded with

and without oxygen, meanwhile, CuO_x enhanced the formation of DMC [26,27]. Our study showed that with increasing the exchange degree, different Cu states were produced, such as Cu^{2+} , Cu^+ , Cu_2O , CuO and CuY zeolites, leading to different catalytic performance [28].

A number of studies investigated the possible reaction schemes of oxidative carbonylation of methanol to DMC on Cu-exchanged zeolite [16,20,22,25,29–31], Pd-exchanged zeolite [9,32], Cu/AC [33], $\gamma\text{-Cu}_2\text{Cl}(\text{OH})_3$ [34], CuCl [35] and Cu_2O [8,36] catalysts. Generally, the molecularly adsorbed methanol is first oxidized by oxygen to methoxide or di-methoxide species. Then the formation of DMC follows two distinct reaction pathways. The first starts with the insertion of CO into methoxide to produce CH_3OCO , which subsequently reacts with CH_3OH to form DMC. The second involves the CO addition to di-methoxide species. Experimental investigation by Engeldinger et al. [26,27] showed that CuO_x aggregates were formed in CuY catalyst when the Cu loading was above 11 wt%, which promoted oxidation and oxocarbonylation reactions of methanol and enhanced the formation of DMC. They suggested that the reaction was closely related to the CH_3OCOOH (MMC), which was produced through participation of lattice oxygen from CuO_x of the catalyst. Cu was reoxidized by gas phase oxygen according to the Mars–van Krevelen mechanism [37]. Although the role of CuO_x has been identified, there is little information on the detailed reaction mechanism which addresses the Cu_2O , CuO and Cu^{2+} species of Y zeolite during oxidative carbonylation of methanol.

In this work, the reaction mechanisms governing oxidative carbonylation of methanol to DMC were studied with Cu^+ , Cu^{2+} , Cu_2O and CuO species in Y zeolites using density functional theory (DFT). An appropriate size of CuY cluster was constructed as the stable configuration, reflecting different Cu states in Y zeolite. Then, the reaction mechanisms for DMC formation on four types of Cu species were investigated, and the order of catalytic activity of different Cu states in Y zeolite was characterized. It is expected that these results will provide a theoretical clue to prepare CuY catalyst with better catalytic activity for the DMC synthesis.

2. Results

A faujasite type structure with various cationic sites and different crystallographic oxygen positions is shown in Figure 1. As reactant molecule, CO is very difficult to diffuse inside the sodalite cages and hexagonal prisms (2.3 Å) [38] of Y zeolite because of the large dynamic diameter (3.76 Å), while they easily enter supercages (7.4 Å) [38], suggesting that only copper species located at sites II and III are accessible to CO adsorption and act as the active sites for the oxidative carbonylation of methanol to DMC. Based on the previous studies [30,31,39,40], copper cations in site II are more stable than site III, therefore site II was selected to represent the location of active center Cu species in this study.

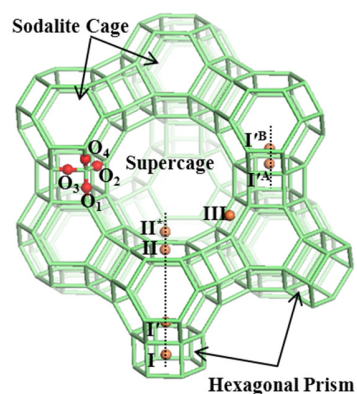


Figure 1. Faujasite type structure with cationic sites (orange balls) and different crystallographic oxygen positions (red balls). Here, site I is at the middle of hexagonal prism; site I'B is in the sodalite cage adjacent to 6MR which is shared by both hexagonal prism and sodalite cage; site I'A is similar to site I'B, but away from the sodalite cage; site II is in the supercage close to the six-membered ring (6 MR) shared by supercage and sodalite cage; site II* is similar to site II, but located towards the supercage; site III is in the supercage that is next to four-membered rings (4 MR) of sodalite cage.

According to the literatures [30,41,42], the local conformation and interactions of molecule can be described using the cluster model. The dangling bonds were saturated by H atoms [41,43]. The terminal H atoms were oriented along the bond direction of Y zeolite. The bond length of O-H was set to 1.0 Å, respectively. During numerical optimization, the local structure of Y zeolite was kept unchanged for Y^{n-} , Y, CuY cluster models. The compensating charges, Al atoms and adjacent SiO_4 units were relaxed, while other atoms were fixed. For the adsorbate-CuY cluster system, the compensating charges, the absorbed molecules and the 6 MR occupied by the active center Cu^+ species were relaxed.

In order to find the appropriate cluster size, five different sized clusters, consisting of 6T, 12T, 24T, 42T, and 60T atoms (T represents an Al or Si atom) (see Figure 2), were constructed.

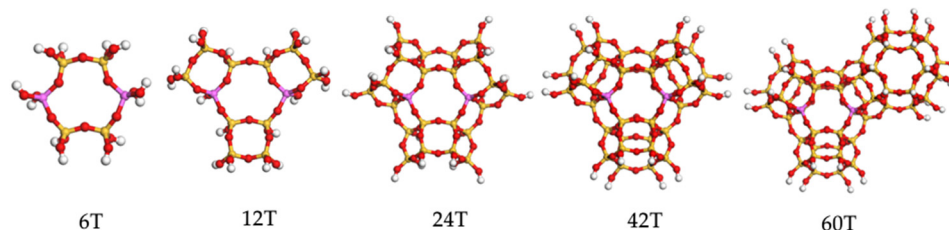


Figure 2. The cluster geometries of Y zeolite with different sizes. Red, yellow, pink and white balls stand for O, Si, Al and H atoms, respectively.

The binding energies of Cu^{2+} in these five Y clusters and the adsorption energies of CO on CuY zeolite with these clusters were calculated, as shown in Table 1.

Table 1. The interaction energies (E_{int}) of Cu^{2+} and the adsorption energies (E_{ads}) of CO on the clusters of Cu^{2+} Y zeolites with different sizes.

| Y Zeolite with Different Size | $E_{int}/kJ \cdot mol^{-1}$ | $E_{ads}/kJ \cdot mol^{-1}$ |
|-------------------------------|-----------------------------|-----------------------------|
| 6T | 2713.62 | 91.45 |
| 12T | 2588.76 | 83.33 |
| 24T | 2529.59 | 83.08 |
| 42T | 2454.44 | 83.27 |
| 60T | 2442.61 | 82.88 |

The interaction energy (E_{int}) between Cu^{2+} and Y^{2-} zeolite was defined as [44]

$$E_{int} = E_{Cu^{2+}} + E_{Y^{2-}} - E_{MY}$$

where $E_{Cu^{2+}}$ is the total energy of Cu^{2+} , $E_{Y^{2-}}$ is the total energy of Y^{2-} , and E_{MY} is the total energy of MY, respectively. Here, a larger E_{int} represents a more stable structure of Cu^{2+} Y system. It can be found from Table 1 that the effect of the cluster size on the adsorption energies of CO is negligible, while the Cu^{2+} interaction energies are significantly influenced by the cluster size. Therefore, a very small cluster model cannot fully reflect the structure of Y zeolite. Comparison of the Cu^{2+} interaction energies suggests that the difference between 24T and 60T cluster is within the allowable error range (<80 kJ/mol). The 24T cluster model was selected in this study to reduce the computing cost.

To better represent the structure of Y zeolite in experiments, four Si atoms of the Y zeolite cluster were substituted by four Al atoms according to the Lowenstein–Dempsey rules. The Y cluster with four Si atoms replaced by Al atoms was denoted as Y^{4-} . Based on the 24T cluster model of Y zeolite, the most stable configurations of Y^{4-} cluster was obtained by evaluating the substitution energy [45] and binding energy of Y^{4-} , which are defined as

$$E_{sub} = E_{Y^{4-}} + 4E_{Si} - E_Y - 4E_{Al}$$

$$E_{bind} = 24E_H + 60E_O + 4E_{Al} + 20E_{Si} - E_{Y^{4-}}$$

where, E_{sub} and E_{bind} are the substitution energy and the binding energy of Y^{4-} , respectively. $E_{Y^{4-}}$ and E_Y are the total energies of Y^{4-} cluster and the Y cluster without the replacement of Si, respectively. E_{Si} , E_{Al} , E_{H} and E_{O} are the energies of single Si, Al, H and O atoms, respectively. With these definitions, a smaller E_{sub} indicates an easier replacement of Si by Al and larger E_{bind} means a more stable Y cluster.

Table 2 lists the calculated E_{sub} and E_{bind} for different distribution of Al atoms.

Table 2. The substitution energies (E_{sub}) and binding energies (E_{bind}) for the Y^{4-} cluster with different distribution of Al atoms.

| The Distribution of Al Atoms | $E_{\text{sub}}/\text{kJ}\cdot\text{mol}^{-1}$ | $E_{\text{bind}}/\text{Ha}$ |
|------------------------------|--|-----------------------------|
| 1-11-12-22 | 27.31 | 21.0454 |
| 2-11-12-22 | 31.16 | 21.0440 |
| 3-11-12-22 | 45.15 | 21.0387 |
| 4-11-12-22 | 0.28 | 21.0557 |
| 5-11-12-22 | 37.72 | 21.0415 |
| 8-11-12-22 | 31.96 | 21.0436 |
| 9-11-12-22 | 122.11 | 21.0093 |
| 11-12-14-22 | 107.60 | 21.0148 |
| 11-12-17-22 | 210.52 | 20.9756 |
| 11-12-20-22 | 129.81 | 21.0064 |
| 11-12-22-24 | 125.49 | 21.0080 |

Due to its least substitution energy and largest binding energy of Y^{4-} , Y^{4-} cluster with the distribution of 4 Al atoms, denoted as 4-11-12-22, is the most stable structure of Y^{4-} cluster (see Figure 3). Negative charges, which are introduced when Si atoms are replaced by Al atoms, are usually compensated by protons associated with crystallographic oxygen atoms adjacent to the Al atoms.

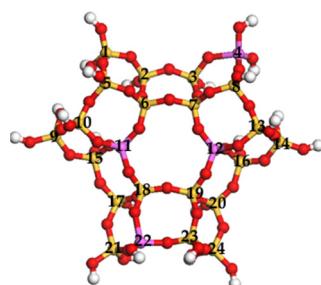


Figure 3. The stable cluster geometry of Y^{4-} zeolite with 24T atoms. See Figure 2 for the color coding.

Based on the stable structure of Y^{4-} cluster, the configurations to reflect the different Cu states in Y zeolite were constructed. According to the literatures [44,46], a majority of charge-compensating protons locate at O1 sites, while the others occupy O3 sites to avoid the formation of $-\text{OH}_2$ group. In this study, for Y zeolite with five Al atoms, three charge-compensating protons locate at O1 sites, and two protons are at O3 sites (see Figure 3). For Cu^{2+}Y zeolite, Cu^{2+} is used to balance the negative charge of Al11 and Al12, and charge-compensating protons are located at the O1 site to balance the negative charges of Al4 and Al22, respectively (see Figure 4a). For Cu^+Y zeolite, Cu^+ balances the negative charge of Al12, when three protons located at the O1 site compensate the negative charges of Al4, Al11 and Al22 (see Figure 4b). For $\text{Cu}_2\text{O-Y}$ and CuO-Y zeolite, all negative charges of Al are compensated by four charge-compensating protons located at O1 and O3 (see Figure 4c,d).

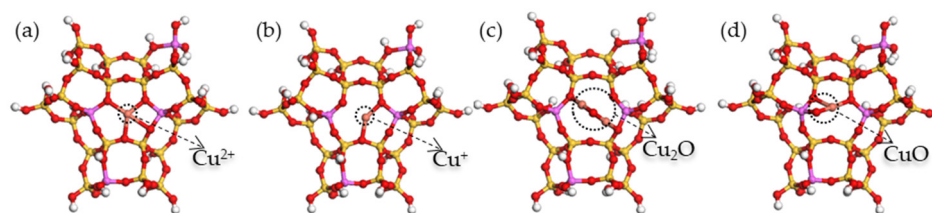


Figure 4. The stable cluster geometries of (a) Cu^{2+}Y , (b) Cu^+Y , (c) $\text{Cu}_2\text{O-Y}$ and (d) CuO-Y zeolites. Red, yellow, pink, white and orange balls stand for O, Si, Al, H and Cu atoms, respectively.

3. Discussion

In this section, the notation $(\text{X})^*$ and $(\text{X})(\text{Y})^*$ are referred to active center Cu states, such as Cu^+ , Cu^{2+} , Cu_2O and CuO interacting with species X and X and Y, respectively. The optimized geometries of reactants, transition states and products for different reaction pathways of DMC formation were calculated.

3.1. The Desorption and Dissociation of CH_3OH

The processes of desorption and dissociation of CH_3OH on these four types of zeolites and the corresponding transition states TS1 are shown in Figure 5.

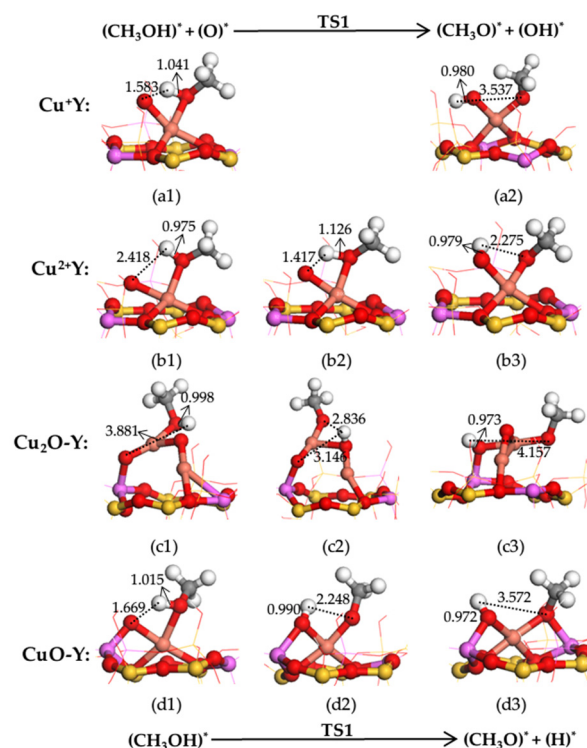


Figure 5. The structures of reactants, products and transition states on Cu^+Y , Cu^{2+}Y , $\text{Cu}_2\text{O-Y}$ and CuO-Y zeolite for the oxidation of CH_3OH to CH_3O (unit: Å). (a1) $(\text{CH}_3\text{OH})^*/(\text{O})^*$ on Cu^+Y , (a2) $(\text{CH}_3\text{O})^*/(\text{OH})^*$ on Cu^+Y , (b1) $(\text{CH}_3\text{OH})^*/(\text{O})^*$ on Cu^{2+}Y , (b2) TS1 on Cu^{2+}Y , (b3) $(\text{CH}_3\text{O})^*/(\text{OH})^*$ on Cu^{2+}Y , (c1) $(\text{CH}_3\text{OH})^*/(\text{O})^*$ on $\text{Cu}_2\text{O-Y}$, (c2) TS1 on $\text{Cu}_2\text{O-Y}$, (c3) $(\text{CH}_3\text{O})^*/(\text{OH})^*$ on $\text{Cu}_2\text{O-Y}$, (d1) $(\text{CH}_3\text{OH})^*/(\text{O})^*$ on CuO-Y , (d2) TS1 on CuO-Y and (d3) $(\text{CH}_3\text{O})^*/(\text{OH})^*$ on CuO-Y . See Figure 4 for the color coding.

As shown in Figure 5, adsorbed CH_3OH on the four types of zeolites are bound to different kinds of active center Cu species through O atom. The adsorption of CH_3OH on Cu^+Y , Cu^{2+}Y , $\text{Cu}_2\text{O-Y}$ and CuO-Y zeolites is exothermic with the energy release of 65.59, 85.81, 122.70 and 94.07 $\text{kJ}\cdot\text{mol}^{-1}$, respectively. Subsequently, for Cu^+Y zeolite, with the presence of oxygen, the O-H bond of CH_3OH breaks to form the co-adsorbed $(\text{CH}_3\text{O})^*(\text{OH})^*$ configuration (see Figure 5(a2)). Since no TS state has been found, molecularly adsorbed CH_3OH

is converted rapidly to CH_3O species. This demonstrates that the presence of adsorbed O on Cu^+Y zeolite exhibits a high surface reactivity toward the formation of CH_3O . The results are in good agreement with early reported experimental observations [15,20,22,28].

For Cu^{2+}Y zeolite, adsorbed CH_3OH is oxidized by adsorbed O to form CH_3O species via a transition state (TS1), as shown in Figure 5(b2). The O-H distance in CH_3OH increases from initial 0.975 Å to 1.126 Å of TS1, and finally to 2.275 Å, showing that the O-H bond in CH_3OH is destroyed. Meanwhile, the distance between adsorbed O atom and H atom decreases drastically from initial 2.418 Å to 1.417 Å of TS1, then to 0.979 Å of $(\text{CH}_3\text{O})^*/(\text{OH})^*$ (see Figure 5(b3)), revealing that a new O-H bond forms on Cu^{2+}Y zeolite. Similar changes are found on $\text{Cu}_2\text{O-Y}$ zeolite. For these two zeolites, the oxidation of adsorbed CH_3OH with the presence of oxygen needs to overcome activation barriers of 66.73 and 23.56 $\text{kJ}\cdot\text{mol}^{-1}$, respectively (see Table 3).

Table 3. The activation barriers for individual reaction steps based on two proposed reaction mechanisms ($\text{kJ}\cdot\text{mol}^{-1}$).

| Catalyst | $(\text{CH}_3\text{OH})^* + \text{O}^* \rightarrow (\text{CH}_3\text{O})^*(\text{OH})^*$ | $(\text{CH}_3\text{O})^* + \text{CO}^* \rightarrow (\text{CH}_3\text{OCO})^*$ | $(\text{CH}_3\text{OCO})^* + (\text{CH}_3\text{O})^* \rightarrow (\text{DMC})^*$ | $(\text{CH}_3\text{O})^*(\text{OH})^* + \text{CH}_3\text{OH} \rightarrow (\text{CH}_3\text{O})_2^* + \text{H}_2\text{O}$ | $(\text{CH}_3\text{O})_2^* + \text{CO} \rightarrow (\text{DMC})^*$ | Ref. |
|--------------------------|--|---|--|--|--|------------|
| Cu_2O | – | 161.9 | 98.8 | 68.3 | 308.5 | [36] |
| $\text{Cu}_2\text{O-Y}$ | 23.56 | 60.01 | 40.90 | 116.38 | 253.96 | This study |
| Cu^+Y | – | 63.73 | 28.27 | 93.86 | 201.68 | This study |
| Cu^{2+}Y | 66.73 | 64.45 | 37.95 | 89.49 | 164.95 | This study |
| CuO-Y | 39.94 | 104.64 | 15.95 | 115.29 | 210.74 | This study |
| CuO | – | 114.5 | 200.9 | 25.7 | 109.1 | [47] |

It is interesting to note that for CuO-Y zeolite, adsorbed CH_3OH is oxidized to CH_3O species without the presence of O, which is attributed to the presence of lattice oxygen from CuO species. Experimental studies by Engeldinger et al. [26,27] suggested that the formation of methoxy species from the adsorbed CH_3OH proceeded with and without oxygen, indicating that lattice oxygen of CuO_x was able to participate in the oxidation process. According to the Mars–van Krevelen mechanism [37], gas phase oxygen can re-oxidize Cu to CuO species [26,27]. These structures in Figure 5 further prove that for the oxidation reaction of CH_3OH to CH_3O , oxygen is needed for $\text{Cu}_2\text{O-Y}$ zeolite but is not essential for CuO-Y zeolite. The oxidation reaction of CH_3OH on CuO-Y zeolite is exothermic ($85.36 \text{ kJ}\cdot\text{mol}^{-1}$) and exhibits an activation barrier of $39.94 \text{ kJ}\cdot\text{mol}^{-1}$, as shown in Table 3.

3.2. Insertion of CO into CH_3O (Path I)

Figure 6 shows the processes of inserting CO into CH_3O to form CH_3OCO on these four types of zeolites and the corresponding transition states TS2.

For Cu^+Y zeolite, the distance between the C atom of CO and the O atom of CH_3O decreases from initially 2.787 Å of $(\text{CO})^*/(\text{CH}_3\text{O})^*$ to 1.961 Å of TS2, which suggests the formation of a new C-O bond. It is also seen from Figure 6 that insertion of CO into Cu-OCH_3 elongates the Cu-O bond from initially 1.901 Å to 2.455 Å of TS2 and then to 2.840 Å of $(\text{CH}_3\text{OCO})^*$, indicating that at the final product CH_3OCO adsorbs on the Cu^+ via the C atom of CO (this C atom is denoted as C' for the further analysis). The CO insertion reaction exhibits an activation barrier of $63.73 \text{ kJ}\cdot\text{mol}^{-1}$ via TS2, which agrees with the results calculated by Zheng et al. [30] (see Table 3). Similar changes from the initial geometries to TS2 states then to the final products happen on the three other types of zeolites. The CO insertion reaction on Cu^{2+}Y , $\text{Cu}_2\text{O-Y}$ and CuO-Y zeolites needs to overcome activation barriers of 64.45, 60.01 and $104.64 \text{ kJ}\cdot\text{mol}^{-1}$, respectively (see Table 3).

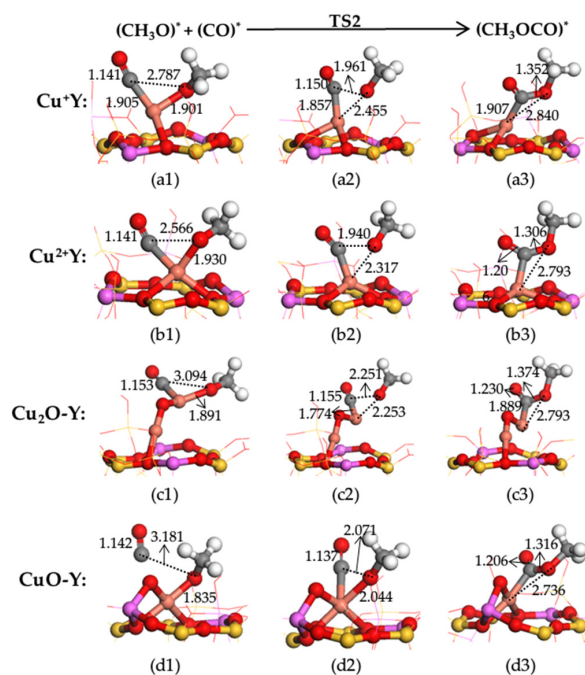


Figure 6. The structures of reactants, products and transition states on Cu^+Y , Cu^{2+}Y , $\text{Cu}_2\text{O-Y}$ and CuO-Y zeolite for the formation of CH_3OCO^* (unit: \AA). (a1) $(\text{CH}_3\text{O})^*/(\text{CO})^*$ on Cu^+Y , (a2) TS2 on Cu^+Y , (a3) $(\text{CH}_3\text{OCO})^*$ on Cu^+Y , (b1) $(\text{CH}_3\text{O})^*/(\text{CO})^*$ on Cu^{2+}Y , (b2) TS2 on Cu^{2+}Y , (b3) $(\text{CH}_3\text{OCO})^*$ on Cu^{2+}Y , (c1) $(\text{CH}_3\text{O})^*/(\text{CO})^*$ on $\text{Cu}_2\text{O-Y}$, (c2) TS2 on $\text{Cu}_2\text{O-Y}$, (c3) $(\text{CH}_3\text{OCO})^*$ on $\text{Cu}_2\text{O-Y}$, (d1) $(\text{CH}_3\text{O})^*/(\text{CO})^*$ on CuO-Y , (d2) TS2 on CuO-Y and (d3) $(\text{CH}_3\text{OCO})^*$ on CuO-Y . See Figure 4 for the color coding.

3.3. CH_3O Reacts with CH_3OCO to Form DMC (Path I)

$(\text{CH}_3\text{OCO})^*$ adsorbed on these four types of zeolites can react with another $(\text{CH}_3\text{O})^*$ to form DMC, via a transition state TS3 (see Figure 7).

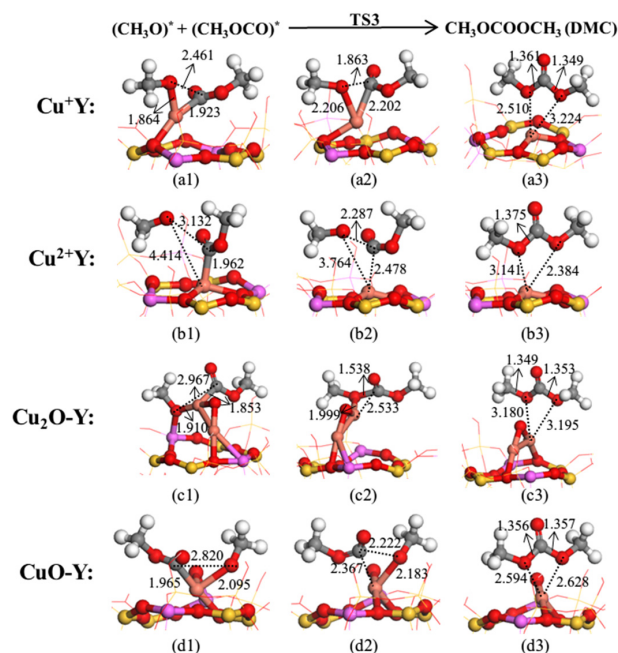


Figure 7. The structures of reactants, products and transition states on Cu^+Y , Cu^{2+}Y , $\text{Cu}_2\text{O-Y}$ and CuO-Y zeolite for the formation of DMC via path I (unit: \AA). (a1) $(\text{CH}_3\text{O})^*/(\text{CH}_3\text{OCO})^*$ on Cu^+Y , (a2) TS3 on Cu^+Y , (a3) DMC on Cu^+Y , (b1) $(\text{CH}_3\text{O})^*/(\text{CH}_3\text{OCO})^*$ on Cu^{2+}Y , (b2) TS3 on Cu^{2+}Y , (b3) DMC on Cu^{2+}Y , (c1) $(\text{CH}_3\text{O})^*/(\text{CH}_3\text{OCO})^*$ on $\text{Cu}_2\text{O-Y}$, (c2) TS3 on $\text{Cu}_2\text{O-Y}$, (c3) DMC on $\text{Cu}_2\text{O-Y}$, (d1) $(\text{CH}_3\text{O})^*/(\text{CH}_3\text{OCO})^*$ on CuO-Y , (d2) TS3 on CuO-Y and (d3) DMC on CuO-Y . See Figure 4 for the color coding.

For Cu^+Y zeolite, the distance between C' atom of $\text{CH}_3\text{OC}'\text{O}$ and the O atom of the second CH_3O (this O atom is denoted as O' for the later analysis) decreases from initially 2.461 Å of $(\text{CH}_3\text{OC}'\text{O})^*/(\text{CH}_3\text{O}')^*$ to 1.863 Å of TS3, and finally the $\text{C}'\text{-O}'$ bond in DMC of 1.361 Å. In addition, the bonds of $\text{Cu}\text{-C}'$ and $\text{Cu}\text{-O}'$ are elongated to 3.433 (not shown in Figure 7) and 2.510 Å, respectively, suggesting the weak (physical) adsorption of DMC on Cu^+Y zeolite. Similar changes from the initial geometries to TS3 states then to the final products happen on the three other types of zeolites. The reaction of CH_3O with CH_3OCO on Cu^+Y , Cu^{2+}Y , $\text{Cu}_2\text{O}\text{-Y}$ and $\text{CuO}\text{-Y}$ zeolites exhibits activation barriers of 28.27, 37.95, 40.90 and 15.95 $\text{kJ}\cdot\text{mol}^{-1}$ via TS3, respectively (see Table 3), and the exothermic energies are 164.16, 315.11, 313.18 and 312.58 $\text{kJ}\cdot\text{mol}^{-1}$, respectively for these four types of zeolites.

3.4. Formation of $(\text{CH}_3\text{O})_2$ Species (Path II)

The second pathway to form DMC suggests that $(\text{CH}_3\text{O})^*/(\text{OH})^*$ reacts with CH_3OH , which results in co-adsorption of $(\text{CH}_3\text{O})_2^*$ and H_2O . Figure 8 shows these adsorption configurations of $(\text{CH}_3\text{O})^*(\text{OH})^*/\text{CH}_3\text{OH}$ and $(\text{CH}_3\text{O})_2^*/\text{H}_2\text{O}$ on these four types of zeolites, via a transition state TS4.

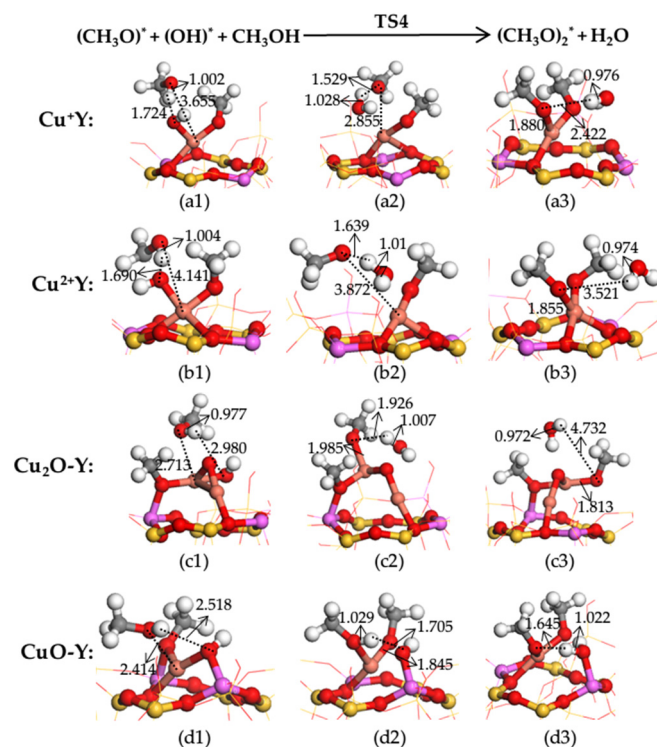


Figure 8. The structures of reactants, products and transition states on Cu^+Y , Cu^{2+}Y , $\text{Cu}_2\text{O}\text{-Y}$ and $\text{CuO}\text{-Y}$ zeolite for the formation of $(\text{CH}_3\text{O})_2$ (unit: Å). (a1) $(\text{CH}_3\text{O})^*/(\text{OH})^*/\text{CH}_3\text{OH}$ on Cu^+Y , (a2) TS4 on Cu^+Y , (a3) $(\text{CH}_3\text{O})_2^*/\text{H}_2\text{O}$ on Cu^+Y , (b1) $(\text{CH}_3\text{O})^*/(\text{OH})^*/\text{CH}_3\text{OH}$ on Cu^{2+}Y , (b2) TS4 on Cu^{2+}Y , (b3) $(\text{CH}_3\text{O})_2^*/\text{H}_2\text{O}$ on Cu^{2+}Y , (c1) $(\text{CH}_3\text{O})^*/(\text{OH})^*/\text{CH}_3\text{OH}$ on $\text{Cu}_2\text{O}\text{-Y}$, (c2) TS4 on $\text{Cu}_2\text{O}\text{-Y}$, (c3) $(\text{CH}_3\text{O})_2^*/\text{H}_2\text{O}$ on $\text{Cu}_2\text{O}\text{-Y}$, (d1) $(\text{CH}_3\text{O})^*/(\text{OH})^*/\text{CH}_3\text{OH}$ on $\text{CuO}\text{-Y}$, (d2) TS4 on $\text{CuO}\text{-Y}$ and (d3) $(\text{CH}_3\text{O})_2^*/\text{H}_2\text{O}$ on $\text{CuO}\text{-Y}$. See Figure 4 for the color coding.

For Cu^+Y zeolite, the O-H distance in CH_3OH increases from initially 1.002 Å to 1.529 Å of TS3, indicating this O-H bond tends to break. Meanwhile, the distance between the H atom of OH in CH_3OH and the O atom of $(\text{OH})^*$ decreases from initially 1.724 Å of $(\text{CH}_3\text{O})^*(\text{OH})^*/\text{CH}_3\text{OH}$ to 1.028 Å of TS4, demonstrating the migration of the H atom away from CH_3OH and towards the O atom of OH. This leads to the formation of additional $(\text{CH}_3\text{O})^*$ and H_2O . Moreover, the distance between the O atom of CH_3OH and Cu^+ decreases from 2.855 Å of TS4 to 1.880 Å of $(\text{CH}_3\text{O})_2^*/\text{H}_2\text{O}$, which suggests the formation of $(\text{CH}_3\text{O})_2^*$. This reaction on Cu^+Y , Cu^{2+}Y , $\text{Cu}_2\text{O}\text{-Y}$ and $\text{CuO}\text{-Y}$ zeolites exhibits activation barriers of 93.86, 89.49, 116.38 and 115.29 $\text{kJ}\cdot\text{mol}^{-1}$ via TS4, respectively (see Table 3).

3.5. Insertion of CO into $(\text{CH}_3\text{O})_2$ to Form DMC (Path II)

The processes of inserting CO into $(\text{CH}_3\text{O})_2$ to form DMC on these four types of zeolites and the corresponding transition states TS5 are shown in Figure 9.

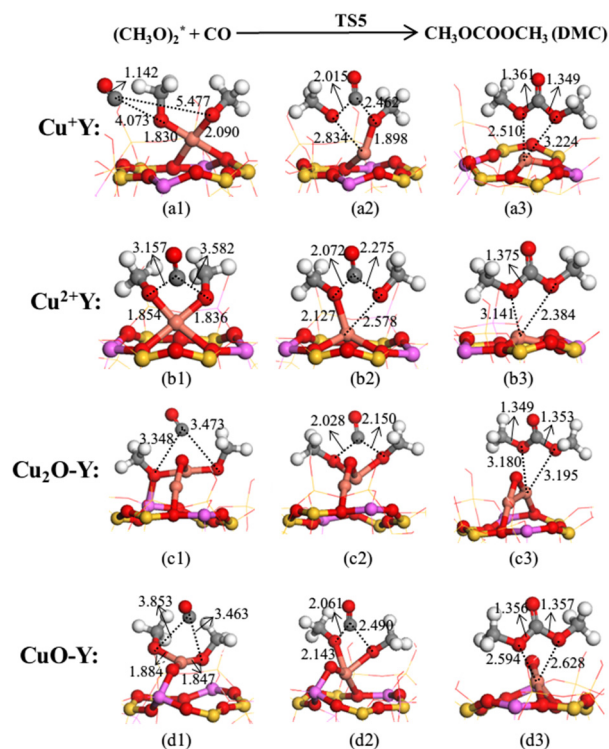


Figure 9. The structures of reactants, products and transition states on Cu^+Y , $\text{Cu}^{2+\text{Y}}$, $\text{Cu}_2\text{O-Y}$ and CuO-Y zeolite for the formation of DMC via path II (unit: Å). (a1) $(\text{CH}_3\text{O})_2^*/\text{CO}$ on Cu^+Y , (a2) TS5 on Cu^+Y , (a3) DMC on Cu^+Y , (b1) $(\text{CH}_3\text{O})_2^*/\text{CO}$ on $\text{Cu}^{2+\text{Y}}$, (b2) TS5 on $\text{Cu}^{2+\text{Y}}$, (b3) DMC on $\text{Cu}^{2+\text{Y}}$, (c1) $(\text{CH}_3\text{O})_2^*/\text{CO}$ on $\text{Cu}_2\text{O-Y}$, (c2) TS5 on $\text{Cu}_2\text{O-Y}$, (c3) DMC on $\text{Cu}_2\text{O-Y}$, (d1) $(\text{CH}_3\text{O})_2^*/\text{CO}$ on CuO-Y , (d2) TS5 on CuO-Y and (d3) DMC on CuO-Y . See Figure 4 for the color coding.

As shown in Figure 9, on Cu^+Y zeolite the distance of Cu-CO of $(\text{CH}_3\text{O})_2^*/\text{CO}$ configuration is 5.477 Å, and the C-O bond (1.142 Å) of CO is similar to that (1.143 Å) of CO in gas phase. This suggests that two CH_3O (i.e., $(\text{CH}_3\text{O})_2^*$) molecules adsorbed at the active center Cu effectively inhibit the adsorption of CO, which agrees with the stronger adsorption of CH_3O than CO ($139.59 \text{ kJ}\cdot\text{mol}^{-1}$ vs. $125.25 \text{ kJ}\cdot\text{mol}^{-1}$). Starting from the adsorption configuration of $(\text{CH}_3\text{O})_2^*/\text{CO}$, the formation of DMC goes through a transition state TS5 (see Figure 9). On Cu^+Y zeolite, the distance of the C atom of CO (denoted as C'') and the O atom of the nearest CH_3O (denotes as O'') decreases from initially 4.073 Å to 2.015 Å of TS5. The distance between C'' and the O atom of the furthest CH_3O (denotes as O''') decreases from initially 5.477 Å of $(\text{CH}_3\text{O})_2^*/\text{CO}$ to 2.462 Å of TS5. Furthermore, in TS5, the distance of Cu-O1 is elongated to 2.834 Å from 1.830 Å of $(\text{CH}_3\text{O})_2^*/\text{CO}$ to accommodate the insertion of CO. Similar calculated results are found on the other three types of zeolites. The reaction step on Cu^+Y , $\text{Cu}^{2+\text{Y}}$, $\text{Cu}_2\text{O-Y}$ and CuO-Y zeolites is significantly exothermic by 256.59, 372.06, 232.24 and 323.77 $\text{kJ}\cdot\text{mol}^{-1}$, and the corresponding activation barriers are 201.68, 164.95, 253.96 and 210.74 $\text{kJ}\cdot\text{mol}^{-1}$ via TS5, respectively (see Table 3).

3.6. Desorption of DMC

Desorption of DMC from Cu^+Y , $\text{Cu}^{2+\text{Y}}$, $\text{Cu}_2\text{O-Y}$ and CuO-Y zeolites is endothermic with the energy input of 24.30, 72.18, 41.31 and 65.69 $\text{kJ}\cdot\text{mol}^{-1}$, respectively. These energies needed are compensable by the exothermic reactions of DMC formation on respective zeolites.

3.7. Rate-Limiting Reactions of DMC Formation

The potential energy curves for two reaction paths are plot in Figure 10.

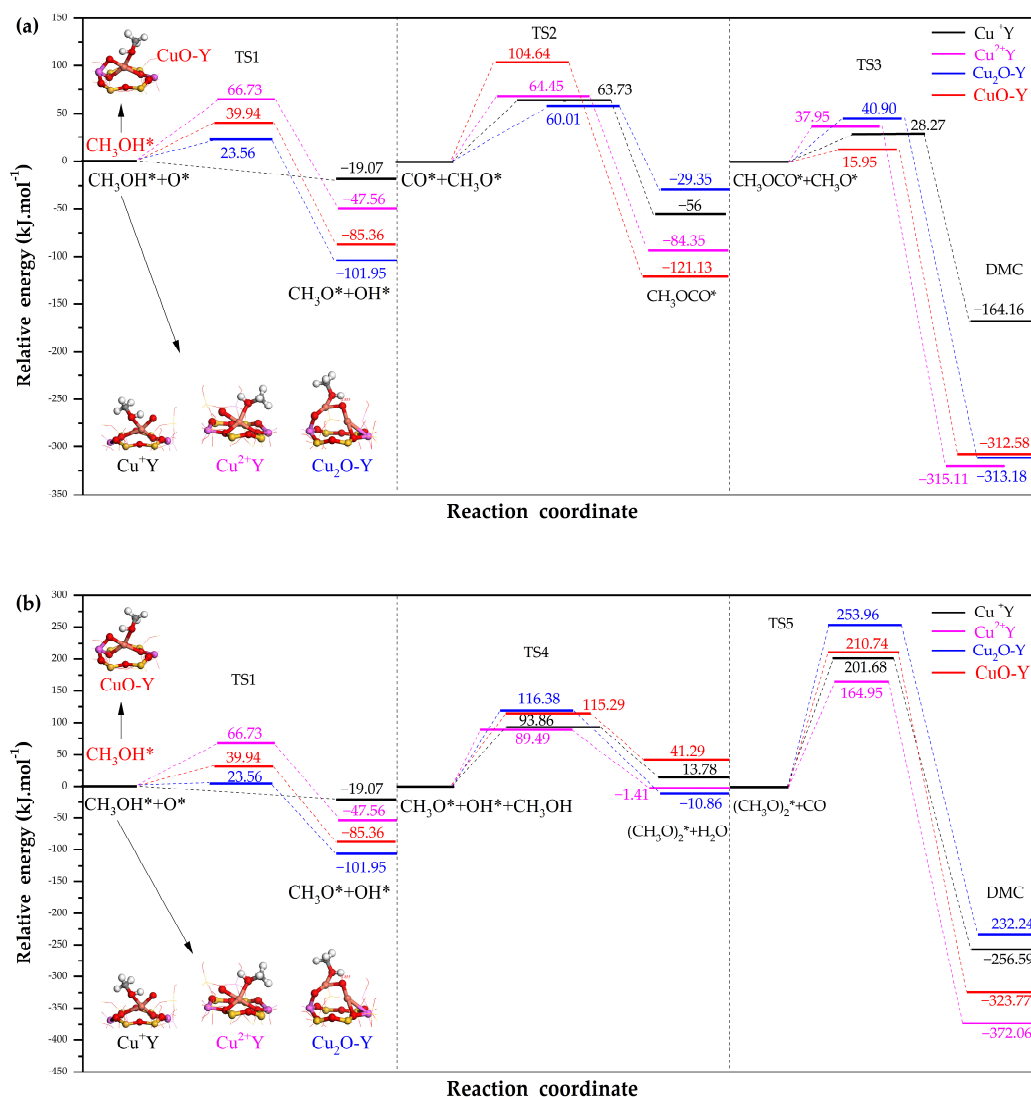


Figure 10. The reaction mechanism for the formation of DMC over Cu⁺Y, Cu₂⁺Y, Cu₂O-Y and CuO-Y zeolites via path I (a) and path II (b).

For the path I of DMC formation on these zeolites, insertion of CO into CH₃O is followed by the formation of DMC. On Cu⁺Y zeolite, the corresponding activation barriers of these two reactions are 63.73 and 28.27 kJ.mol⁻¹, respectively, which suggests the insertion reaction of CO into CH₃O is rate-limiting. On the other hand, for path II of DMC formation, insertion of CO into (CH₃O)₂ is followed by the formation of DMC. On Cu⁺Y zeolite, the rate-limiting step for path II is insertion of CO into (CH₃O)₂ with an activation barrier of 201.68 kJ.mol⁻¹. The comparison between the rate-limiting reactions of two paths (63.73 vs. 201.68 kJ.mol⁻¹) suggests the path I is favorable for DMC formation on Cu⁺Y zeolite. Similar to these processes on Cu⁺Y zeolite, DFT calculations further confirm that path I is the favorable process of DMC formation over CuO-Y and Cu₂O-Y zeolites, with the rate-limiting step of inserting CO into CH₃O. For Cu₂⁺Y zeolite, the favorable pathway of DMC formation is also path I, while oxidation of the absorbed CH₃OH to CH₃O becomes rate-limiting. Zhang et al. [36] found the favorable pathway of DMC formation on Cu₂O(111) follows path I, which agrees with the finding in this study. However, they found that path II was favorable for the formation of DMC over

CuO(111) and the insertion of CO into (CH₃O)₂ was considered as rate-limiting step [47]. Comparison of the activation barriers of the rate-limiting steps on Cu₂O-Y (this study) and Cu₂O(111) (in the literature [36]) (60.01 kJ·mol⁻¹ and 161.9 kJ·mol⁻¹, respectively) suggest the Cu₂O species in Y zeolite should exhibit a better catalytic activity than the carrier-free Cu₂O crystalline surface (see Table 3). These results indicate that the carrier significantly affects the activation barriers and even the reaction pathways.

Based on the aforementioned analyses, the following reaction route of DMC formation on different Cu states in Y zeolites was proposed. First, the adsorbed CH₃OH is oxidized to CH₃O species on zeolites. Then CO inserts to CH₃O to form CH₃OCO, which subsequently reacts with CH₃O to form DMC at a relative high reaction rate. Finally, adsorbed DMC is released into the gas phase. A distinction exists for these four types of zeolites investigated in this study. It is found that the rate-limiting step on Cu²⁺Y zeolite is oxidation of CH₃OH to CH₃O, while for Cu⁺Y, Cu₂O-Y and CuO-Y zeolites, the rate-limiting step is insertion of CO into CH₃O. Moreover, oxidation of CH₃OH to form CH₃O requires a presence of oxygen on Cu⁺Y, Cu²⁺Y and Cu₂O-Y zeolites, while on CuO-Y zeolite the adsorbed CH₃OH is oxidized by the lattice oxygen of CuO. The latter agrees with experimental findings by Engeldinger et al. [26,27].

The activation barriers of insertion of CO into CH₃O over Cu⁺Y, Cu²⁺Y, Cu₂O-Y and CuO-Y zeolites are found to be 63.73, 64.45, 60.01 and 104.64 kJ·mol⁻¹, respectively. Worthwhile to notice, oxidation of CH₃OH to CH₃O on Cu²⁺Y zeolite exhibits an activation barrier of 66.73 kJ·mol⁻¹, while oxidation of CH₃OH on Cu⁺Y zeolite is a barrier free reaction, suggesting that Cu⁺Y zeolite possess a better catalytic activity than Cu²⁺Y zeolite. As a result, the order of catalytic activities of these four types of zeolites is derived as Cu₂O-Y ≈ Cu⁺Y > Cu²⁺Y > CuO-Y, which agrees with a previous experimental study [28].

4. Methodology

Density functional theory calculations were performed using the DMol³ program package of Materials Studio 8.0 [48]. The generalized-gradient approximation (GGA) with the Perdew–Burke–Ernzerhof (PBE) exchange-correction functional was used in all calculations [49]. The double numerical plus polarization (DNP) basis set [50], which is equivalently accurate to the commonly used 6-31G** Gaussian basis set, was employed to describe the Si-O-H-Al-Cu system. In this approach, for the non-metal Si, O, H and C atoms were treated with the all-electron basis sets, which considers all valence orbitals, while the inner electrons of the Al and Cu atoms were kept frozen and replaced by an effective core potential (ECP), which is attributed to that the metal atom participated into the reaction mainly occurs by the outer valence electron orbitals. The convergence criteria of DFT calculations were set to 2×10^{-5} Ha for energy, 4×10^{-3} Ha/Å for force, 0.005 Å for displacement. Complete linear synchronous transit (LST) and quadratic synchronous transit (QST) were used to determine the transition states (TS).

For the reaction $A + B \rightarrow AB$ on CuY zeolite, the reaction enthalpy (ΔH) and activation energy (E_a) were calculated by

$$\Delta H = E_{AB/CuY} - E_{A+B/CuY}$$

$$E_a = E_{TS/CuY} - E_{A+B/CuY}$$

where $E_{AB/CuY}$ is the total energy for the product AB on CuY zeolite, $E_{A+B/CuY}$ is the total energies of the co-adsorbed A and B on CuY zeolite and $E_{TS/CuY}$ is the total energy of the transition state (TS) on CuY zeolite, respectively. The negative ΔH represents an exothermic reaction.

The adsorption energy (E_{ads}) of the adsorbate-cluster system is defined as

$$E_{ads} = E_{adsorbate} + E_{CuY} - E_{adsorbate/CuY}$$

where $E_{\text{adsorbate/CuY}}$ is the total energy of adsorbate-CuY substrate system in the equilibrium state, E_{CuY} and $E_{\text{adsorbate}}$ are the total energies of CuY substrate and free adsorbate alone, respectively. From this definition, the large adsorption energy indicates a strong interaction between the adsorbate and CuY zeolite.

5. Conclusions

In this work, the DFT method was employed to investigate the reaction mechanisms of DMC formation on four types of zeolites doped with Cu^+ , Cu^{2+} , Cu_2O and CuO , respectively, based on two proposed reaction pathways. The calculation results reveal that path I is dominant for the formation of DMC since the activation barriers of rate-limiting steps for path II are much higher than that of path I. Moreover, the calculation results also suggest the following route to describe DMC formation on these zeolites. First, CH_3OH is adsorbed and oxidized to CH_3O species. Then CO inserts into CH_3O to form CH_3OCO , which reacts with CH_3O to product DMC. Lastly, adsorbed DMC is released into the gas phase. It is found that for Cu^+Y , Cu^{2+}Y and $\text{Cu}_2\text{O}\text{-Y}$ zeolites, adsorbed CH_3OH is oxidized to CH_3O with a presence of oxygen, whereas oxidation of CH_3OH on $\text{CuO}\text{-Y}$ utilizes the lattice oxygen of CuO . The rate-limiting step on Cu^{2+}Y zeolite is oxidation of CH_3OH to CH_3O , while on three other types of zeolites, the rate-limiting step is insertion of CO into CH_3O , and the corresponding activation barriers of these rate-limiting steps for Cu^{2+}Y , Cu^+Y , $\text{Cu}_2\text{O}\text{-Y}$ and $\text{CuO}\text{-Y}$ zeolites are 66.73, 63.73, 60.01 and 104.64 $\text{kJ}\cdot\text{mol}^{-1}$, respectively. Based on above mentioned, the catalytic activities of these four types of zeolites with different Cu states exhibit the order of $\text{Cu}_2\text{O}\text{-Y} \approx \text{Cu}^+\text{Y} > \text{Cu}^{2+}\text{Y} > \text{CuO}\text{-Y}$. These findings are expected to guide the selection and preparation of CuY catalysts with the best catalytic activity for DMC synthesis.

Author Contributions: H.Z. and S.Y. outlined the work plan; Y.Z. and Y.S. conducted the computations; Y.Z. and G.Z. drew the figures and drafted the manuscript. H.Z. and J.Z. revised the drafted manuscript. All authors have read and agreed to the published version of the manuscript.

Funding: This work was supported by the National Natural Science Foundation of China (22262020), Zunyi Technology and Big data Bureau, Moutai institute Joint Science and Technology Research and Development Project ([2021]328) and Research Foundation for Scientific Scholars of Moutai Institute (mygccrc[2022]081 and [2022]080).

Data Availability Statement: All the relevant data used in this study have been provided in the form of figures and tables in the published article, and all data provided in the present manuscript are available to whom they may concern.

Acknowledgments: The authors are grateful to Zhong Li, John Z. Wen and Nilesh Narkhede for their kindly academic discussion and language help.

Conflicts of Interest: The authors declare no conflict of interest.

References

1. Kohli, K.; Sharma, B.K.; Panchal, C.B. Dimethyl Carbonate: Review of Synthesis Routes and Catalysts Used. *Energies* **2022**, *15*, 5133. [[CrossRef](#)]
2. Shi, D.; Heyte, S.; Capron, M.; Paul, S. Catalytic processes for the direct synthesis of dimethyl carbonate from CO_2 and methanol: A review. *Green Chem.* **2022**, *24*, 1067–1089. [[CrossRef](#)]
3. Raza, A.; Ikram, M.; Guo, S.; Baiker, A.; Li, G. Green Synthesis of Dimethyl Carbonate from CO_2 and Methanol: New Strategies and Industrial Perspective. *Adv. Sustain. Syst.* **2022**, *6*, 2200087. [[CrossRef](#)]
4. Huo, L.; Wang, T.; Xuan, K.; Li, L.; Pu, Y.; Li, C.; Qiao, C.; Yang, H.; Bai, Y. Synthesis of Dimethyl Carbonate from CO_2 and Methanol over Zr-Based Catalysts with Different Chemical Environments. *Catalysts* **2021**, *11*, 710. [[CrossRef](#)]
5. Ohno, H.; Ikhlal, M.; Tamura, M.; Nakao, K.; Suzuki, K.; Morita, K.; Kato, Y.; Tomishige, K.; Fukushima, Y. Direct dimethyl carbonate synthesis from CO_2 and methanol catalyzed by CeO_2 and assisted by 2-cyanopyridine: A cradle-to-gate greenhouse gas emission study. *Green Chem.* **2021**, *23*, 457–469. [[CrossRef](#)]
6. Liu, K.; Liu, C. Synthesis of dimethyl carbonate from methanol and CO_2 under low pressure. *RSC Adv.* **2021**, *11*, 35711–35717. [[CrossRef](#)] [[PubMed](#)]
7. Huang, S.; Yan, B.; Wang, S.; Ma, X. Recent advances in dialkyl carbonates synthesis and applications. *Chem. Soc. Rev.* **2015**, *44*, 3079–3116. [[CrossRef](#)]

8. Wang, J.; Fu, T.; Meng, F.; Zhao, D.; Chuang, S.S.C.; Li, Z. Highly active catalysis of methanol oxidative carbonylation over nano Cu₂O supported on micropore-rich mesoporous carbon. *Appl. Catal. B Environ.* **2022**, *303*, 120890. [[CrossRef](#)]
9. Wang, C.; Liu, B.; Liu, P.; Huang, K.; Xu, N.; Guo, H.; Bai, P.; Ling, L.; Liu, X.; Mintova, S. Elucidation of the reaction mechanism of indirect oxidative carbonylation of methanol to dimethyl carbonate on Pd/NaY catalyst: Direct identification of reaction intermediates. *J. Catal.* **2022**, *412*, 30–41. [[CrossRef](#)]
10. Al-Rabiah, A.A.; Almutlaq, A.M.; Bashth, O.S.; Alyasser, T.M.; Alshehri, F.A.; Alofai, M.S.; Alshehri, A.S. An Intensified Green Process for the Coproduction of DMC and DMO by the Oxidative Carbonylation of Methanol. *Processes* **2022**, *10*, 2094. [[CrossRef](#)]
11. Almusaiteer, K.A.; Al-Mayman, S.I.; Mamedov, A.; Al-Zeghayer, Y.S. In Situ IR Studies on the Mechanism of Dimethyl Carbonate Synthesis from Methanol and Carbon Dioxide. *Catalysts* **2021**, *11*, 517. [[CrossRef](#)]
12. Zhang, Z.; Che, H.; Wang, Y.; Gao, J.; Ping, Y.; Zhong, Z.; Su, F. Template-free synthesis of Cu@Cu₂O core-shell microspheres and their application as copper-based catalysts for dimethyldichlorosilane synthesis. *Chem. Eng. J.* **2012**, *211–212*, 421–431. [[CrossRef](#)]
13. Ai, Z.; Zhang, L.; Lee, S.; Ho, W. Interfacial Hydrothermal Synthesis of Cu@Cu₂O Core-Shell Microspheres with Enhanced Visible-Light-Driven Photocatalytic Activity. *J. Phys. Chem. C* **2009**, *113*, 20896–20902. [[CrossRef](#)]
14. Teng, F.; Yao, W.; Zheng, Y.; Ma, Y.; Teng, Y.; Xu, T.; Liang, S.; Zhu, Y. Synthesis of flower-like CuO nanostructures as a sensitive sensor for catalysis. *Sensors Actuators B Chem.* **2008**, *134*, 761–768. [[CrossRef](#)]
15. Anderson, S.A.; Root, T.W. Investigation of the effect of carbon monoxide on the oxidative carbonylation of methanol to dimethyl carbonate over Cu+X and Cu+ZSM-5 zeolites. *J. Mol. Catal. A Chem.* **2004**, *220*, 247–255. [[CrossRef](#)]
16. Shen, Y.; Meng, Q.; Huang, S.; Wang, S.; Gong, J.; Ma, X. Reaction mechanism of dimethyl carbonate synthesis on Cu/ β zeolites: DFT and AIM investigations. *RSC Adv.* **2012**, *2*, 7109–7119. [[CrossRef](#)]
17. Zhang, G.; Liang, J.; Yin, J.; Yan, L.; Narkhede, N.; Zheng, H.; Li, Z. An efficient strategy to improve the catalytic activity of CuY for oxidative carbonylation of methanol: Modification of NaY by H4EDTA-NaOH sequential treatment. *Micropor. Mesopor. Mater.* **2020**, *307*, 110500. [[CrossRef](#)]
18. Wang, Y.; Liu, Z.; Tan, C.; Sun, H.; Li, Z. High catalytic activity of CuY catalysts prepared by high temperature anhydrous interaction for the oxidative carbonylation of methanol. *RSC Adv.* **2020**, *10*, 3293–3300. [[CrossRef](#)]
19. Zhang, Y.H.; Briggs, D.N.; De Smit, E.; Bell, A.T. Effects of zeolite structure and composition on the synthesis of dimethyl carbonate by oxidative carbonylation of methanol on Cu-exchanged Y, ZSM-5, and Mordenite. *J. Catal.* **2007**, *251*, 443–452. [[CrossRef](#)]
20. King, S.T. Reaction Mechanism of Oxidative Carbonylation of Methanol to Dimethyl Carbonate in Cu-Y Zeolite. *J. Catal.* **1996**, *161*, 530–538. [[CrossRef](#)]
21. Richter, M.; Fait, M.J.G.; Eckelt, R.; Schneider, M.; Radnik, J.; Heidemann, D.; Fricke, R. Gas-phase carbonylation of methanol to dimethyl carbonate on chloride-free Cu-precipitated zeolite Y at normal pressure. *J. Catal.* **2007**, *245*, 11–24. [[CrossRef](#)]
22. Zhang, Y.H.; Bell, A.T. The mechanism of dimethyl carbonate synthesis on Cu-exchanged zeolite Y. *J. Catal.* **2008**, *255*, 153–161. [[CrossRef](#)]
23. Huang, S.Y.; Wang, Y.; Wang, Z.Z.; Yan, B.; Wang, S.P.; Gong, J.L.; Ma, X.B. Cu-doped zeolites for catalytic oxidative carbonylation: The role of Brønsted acids. *Appl. Catal. A Gen.* **2012**, *417–418*, 236–242. [[CrossRef](#)]
24. Kieger, S.; Delahay, G.; Coq, B.; Neveu, B. Selective Catalytic Reduction of Nitric Oxide by Ammonia over Cu-FAU Catalysts in Oxygen-Rich Atmosphere. *J. Catal.* **1999**, *183*, 267–280. [[CrossRef](#)]
25. Richter, M.; Fait, M.J.G.; Eckelt, R.; Schreier, E.; Schneider, M.; Pohl, M.-M.; Fricke, R. Oxidative gas phase carbonylation of methanol to dimethyl carbonate over chloride-free Cu-impregnated zeolite Y catalysts at elevated pressure. *Appl. Catal. B Environ.* **2007**, *73*, 269–281. [[CrossRef](#)]
26. Engeldinger, J.; Domke, C.; Richter, M.; Bentrup, U. Elucidating the role of Cu species in the oxidative carbonylation of methanol to dimethyl carbonate on CuY: An in situ spectroscopic and catalytic study. *Appl. Catal. A Gen.* **2010**, *382*, 303–311. [[CrossRef](#)]
27. Engeldinger, J.; Richter, M.; Bentrup, U. Mechanistic investigations on dimethyl carbonate formation by oxidative carbonylation of methanol over a CuY zeolite: An operando SSITKA/DRIFTS/MS study. *Phys. Chem. Chem. Phys.* **2012**, *14*, 2183–2191. [[CrossRef](#)]
28. Zheng, H.-Y.; Wang, J.-Z.; Li, Z.; Yan, L.-F.; Wen, J.Z. Characterization and assessment of an enhanced CuY catalyst for oxidative carbonylation of methanol prepared by consecutive liquid-phase ion exchange and incipient wetness impregnation. *Fuel Process. Technol.* **2016**, *152*, 367–374. [[CrossRef](#)]
29. Anderson, S.A.; Root, T.W. Kinetic studies of carbonylation of methanol to dimethyl carbonate over Cu⁺X zeolite catalyst. *J. Catal.* **2003**, *217*, 396–405. [[CrossRef](#)]
30. Zheng, X.B.; Bell, A.T. A Theoretical Investigation of Dimethyl Carbonate Synthesis on Cu⁻Y Zeolite. *J. Phys. Chem. C* **2008**, *112*, 5043–5047. [[CrossRef](#)]
31. Zheng, H.; Qi, J.; Zhang, R.; Li, Z.; Wang, B.; Ma, X. Effect of environment around the active center Cu⁺ species on the catalytic activity of CuY zeolites in dimethyl carbonate synthesis: A theoretical study. *Fuel Process. Technol.* **2014**, *128*, 310–318. [[CrossRef](#)]
32. Shen, Y.; Meng, Q.; Huang, S.; Gong, J.; Ma, X. DFT investigations for the reaction mechanism of dimethyl carbonate synthesis on Pd(ii)/ β zeolites. *Phys. Chem. Chem. Phys.* **2013**, *15*, 13116–13127. [[CrossRef](#)] [[PubMed](#)]
33. Ren, J.; Wang, W.; Wang, D.; Zuo, Z.; Lin, J.; Li, Z. A theoretical investigation on the mechanism of dimethyl carbonate formation on Cu/AC catalyst. *Appl. Catal. A Gen.* **2014**, *472*, 47–52. [[CrossRef](#)]
34. Meng, Q.; Wang, Z.; Shen, Y.; Yan, B.; Wang, S.; Ma, X. DFT and DRIFTS studies of the oxidative carbonylation of methanol over γ -Cu₂Cl(OH)₃: The influence of Cl. *RSC Adv.* **2012**, *2*, 8752–8761. [[CrossRef](#)]

35. Zheng, H.; Zhang, R.; Li, Z. Theoretical Studies on the Interaction of CO and CH₃O on CuCl (111) Surface for Methanol Oxidative Carbonylation. *Chem. J. China Univ.* **2014**, *35*, 1926–1932.
36. Zhang, R.G.; Song, L.Z.; Wang, B.J.; Li, Z. A density functional theory investigation on the mechanism and kinetics of dimethyl carbonate formation on Cu₂O catalyst. *J. Comput. Chem.* **2012**, *33*, 1101–1110. [[CrossRef](#)]
37. Doornkamp, C.; Ponec, V. The universal character of the Mars and Van Krevelen mechanism. *J. Mol. Catal. A Chem.* **2000**, *162*, 19–32. [[CrossRef](#)]
38. Sherry, H.S. The Ion-Exchange Properties of Zeolites. I. Univalent Ion Exchange in Synthetic Faujasite. *J. Phys. Chem.* **1966**, *70*, 1158–1168. [[CrossRef](#)]
39. Zheng, H.; Narkhede, N.; Zhang, G.; Li, Z. Role of metal co-cations in improving CuY zeolite performance for DMC synthesis: A theoretical study. *Appl. Organomet. Chem.* **2020**, *34*, e5832. [[CrossRef](#)]
40. Berthomieu, D.; Duc  r  , J.-M.; Goursot, A. A Theoretical Study of Cu(II) Sites in a Faujasite-Type Zeolite: Structures and Electron Paramagnetic Resonance Hyperfine Coupling Constants. *J. Phys. Chem. B* **2002**, *106*, 7483–7488. [[CrossRef](#)]
41. Drake, I.J.; Zhang, Y.H.; Briggs, D.; Lim, B.; Chau, T.; Bell, A.T. The Local Environment of Cu⁺ in Cu⁺-Y Zeolite and Its Relationship to the Synthesis of Dimethyl Carbonate. *J. Phys. Chem. B* **2006**, *110*, 11654–11664. [[CrossRef](#)] [[PubMed](#)]
42. Zhang, R.; Li, J.; Wang, B. The effect of Si/Al ratios on the catalytic activity of CuY zeolites for DMC synthesis by oxidative carbonylation of methanol: A theoretical study. *RSC Adv.* **2013**, *3*, 12287–12298. [[CrossRef](#)]
43. Yang, G.; Wang, Y.; Zhou, D.; Liu, X.; Han, X.; Bao, X. Density functional theory calculations on various M/ZSM-5 zeolites: Interaction with probe molecule H₂O and relative hydrothermal stability predicted by binding energies. *J. Mol. Catal. A Chem.* **2005**, *237*, 36–44. [[CrossRef](#)]
44. Rejmak, P.; Sierka, M.; Sauer, J. Theoretical studies of Cu(i) sites in faujasite and their interaction with carbon monoxide. *Phys. Chem. Chem. Phys.* **2007**, *9*, 5446–5456. [[CrossRef](#)]
45. Campana, L.; Selloni, A.; Weber, J.; Goursot, A. Cation Siting and Dynamical Properties of Zeolite Offretite from First-Principles Molecular Dynamics. *J. Phys. Chem. B* **1997**, *101*, 9932–9939. [[CrossRef](#)]
46. Hill, J.-R.; Freeman, C.M.; Delley, B. Bridging Hydroxyl Groups in Faujasite: Periodic vs. Cluster Density Functional Calculations. *J. Phys. Chem. A* **1999**, *103*, 3772–3777. [[CrossRef](#)]
47. Kang, L.; Zhang, J.; Zhang, R.; Ling, L.; Wang, B. Insight into the formation mechanism and kinetics for the oxidative carbonylation of methanol to dimethyl carbonate over CuO catalyst: Effects of Cu valence state and solvent environment. *Mol. Catal.* **2018**, *449*, 38–48. [[CrossRef](#)]
48. Delley, B. From molecules to solids with the DMol3 approach. *J. Chem. Phys.* **2000**, *113*, 7756–7764. [[CrossRef](#)]
49. Perdew, J.P.; Burke, K.; Ernzerhof, M. Generalized gradient approximation made simple. *Phys. Rev. Lett.* **1996**, *77*, 3865–3868. [[CrossRef](#)] [[PubMed](#)]
50. Delley, B. An all-electron numerical method for solving the local density functional for polyatomic molecules. *J. Chem. Phys.* **1990**, *92*, 508–517. [[CrossRef](#)]

Disclaimer/Publisher’s Note: The statements, opinions and data contained in all publications are solely those of the individual author(s) and contributor(s) and not of MDPI and/or the editor(s). MDPI and/or the editor(s) disclaim responsibility for any injury to people or property resulting from any ideas, methods, instructions or products referred to in the content.